JOURNAL OF SOLID STATE CHEMISTRY 80, 266–275 (1989)

Anisotropic Electronic Properties of the Diphosphate Tungsten Bronzes $K_2P_8W_{24}O_{88}$, $K_2P_8W_{28}O_{100}$ and Their Substituted Compounds

ENOCH WANG AND MARTHA GREENBLATT

Department of Chemistry, Rutgers, The State University of New Jersey, New Brunswick, New Jersey 08903

IDRIS EL-IDRISSI RACHIDI AND ENRIC CANADELL

Laboratoire de Chimie Théorique, Université de Paris-Sud, 91405 Orsay, France

AND MYUNG-HWAN WHANGBO

Department of Chemistry, North Carolina State University, Raleigh, North Carolina 27695-8204

Received November 17, 1988; in revised form February 28, 1989

Electronic properties of single crystals of $K_2P_8W_{24}O_{88}$ and $K_2P_8W_{28}O_{100}$, the sixth and seventh members of the potassium diphosphate tungsten bronze series $K_x(P_2O_4)_4(WO_3)_{4m}$, were studied. Temperature-dependent resistivity measurements on oriented single crystals reveal quasi-two-dimensional metallic behavior with room-temperature resistivities of $\rho_{a^*} = 5.4 \times 10^{-3}$, $\rho_b = 1.2 \times 10^{-4}$, and $\rho_{c^*} = 3.9 \times 10^{-4}$ Ω cm in $K_2P_8W_{24}O_{88}$ and $\rho_{a^*} = 8.9 \times 10^{-3}$, $\rho_b = 1.5 \times 10^{-4}$, and $\rho_{c^*} = 3.4 \times 10^{-4}$ Ω cm in $K_2P_8W_{28}O_{100}$. Magnetic susceptibility measurements indicate Pauli paramagnetic behavior. In agreement with the above results band electronic calculations on a $W_{24}O_{84}$ slab of $Rb_{1.8}P_8W_{24}O_{88}$ (isostructural with $K_2P_8W_{24}O_{88}$) and a $W_{28}O_{96}$ slab found in $Rb_{1.74}P_8W_{28}O_{100}$ show that the Fermi level cuts both one- and two-dimensional bands, and the conductivity is greater along the *b* axis. Solid-state insertion of Co^{2+}, Fe^{2+}, and Sn^{2+} ions into $K_2P_8W_{24}O_{88}$ and partial substitution of K^+ by alkali metal ions Li^+, Na^+, and Rb^+, respectively, in $K_2P_8W_{24}O_{88}$ lead to an enhancement of the conductivity and an increase in the extent of the anisotropy. For $K_xA_yP_8W_{24}O_{88}$ with A = Li and Na, single crystals form with the monophosphate tungsten bronze structure with pentagonal tunnels rather than the diphosphate tungsten bronze structure with hexagonal cavities as observed for the host compound. Partial substitution of W by Mo in $K_2P_8W_{24}O_{88}$ results in the intergrowth of $K_2P_8W_{24-x}Mo_xO_{88}$ and $K_2P_8W_{28-x}Mo_xO_{100}$. The electronic properties of the Mo-substituted phases change gradually from metal to semiconductor with increasing Mo content.

Introduction

Electronic properties of the ternary tungsten bronzes A_xWO_3 (A = Na (*1*), K (*2*), Rb (*3*), Cs (*4*)) have been studied extensively. The K_xWO_3 and Rb_xWO_3 bronzes exhibit anomalous transport behavior associated with the order–disorder of the A cation (*2*, *3*). Closely related to the tungsten bronzes are the diphosphate tungsten bronzes (DPTB), $A_x(P_2O_4)_4(WO_3)_{4m}$ (A = K with m = 5–11 (*5*); Rb with m = 4–11 (*5*, *6*); Tl

0022-4596/89 $3.00

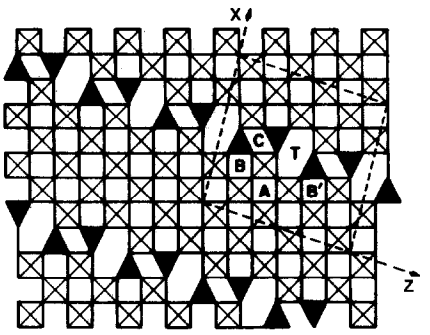

FIG. 1. Structure of the diphosphate tungsten bronzes (DPTB), $A_x(P_2O_4)_4(WO_3)_{4m}$ with $m = 8$.

with $m = 8$ (*7*); Ba with $m = 6$–10 (*8*)). The structure of the diphosphate tungsten bronzes is built up from slabs of ReO_3-type corner-sharing WO_6 octahedra. The slabs of WO_6 octahedra share corners on both sides with P_2O_7 diphosphate groups, creating hexagonal tunnels (hence the designation $DPTB_h$) in forming a three-dimensional network structure. The *A* cations are located in the hexagonal tunnels (Fig. 1). Homologous series of $DPTB_h$ can be synthesized by varying the widths of the slabs (i.e., the magnitude of *m*). The nature of the *A* ion has little influence on the structure of the $DPTB_h$. For monovalent ions with $A = K^+$, Rb^+, and Tl^+ the structural properties of the $DPTB_h$ are nearly identical. Since the slabs of WO_6 octahedra are terminated on both sides by the insulating P_2O_7 groups, the $DPTB_h$ are expected to be quasi-two-dimensional (2D) conductors. Raveau and co-workers (*7*) have studied the electronic properties of polycrystalline $DPTB_h$ and have shown that these bronzes are metallic with their electrical transport properties independent of the nature of the *A* cation. In this paper, we report results of electronic transport and magnetic measurements on oriented single crystals of the sixth and seventh members of potassium $DPTB_h$, $K_2P_8W_{24}O_{88}$ and $K_2P_8W_{28}O_{100}$, which indicate anisotropic, quasi-low-dimensional behavior. To study the effects of substitution on the electronic properties, we investigated the partial substitutions of the K^+ by Li^+, Na^+, and Rb^+ and W by Mo, and also insertion by Fe^{2+}, Sn^{2+}, and Co^{2+} ions.

Finally tight-binding band electronic structure calculations (*9*) were performed on a $W_{24}O_{84}$ slab found in $Rb_{1.8}P_8W_{24}O_{88}$ (isostructural with $K_2P_8W_{24}O_{88}$) and a $W_{28}O_{96}$ slab found in $Rb_{1.74}P_8W_{28}O_{100}$ within the framework of the extended Hückel method (*1*). The atomic parameters employed in our calculations were taken from our previous work (*12*).

Experiment

Polycrystalline specimens of the potassium $DPTB_h$ series with $m = 5$–11 were synthesized from a mixture of $(NH_4)_2HPO_4$, K_2CO_3, WO_3, and W powder in evacuated quartz tubes by solid-state procedures as described earlier (*5*). Reagent grade starting materials $(NH_4)_2HPO_4$, K_2CO_3, and WO_3 were mixed stoichiometrically and first decomposed at 650°C overnight. An appropriate amount of W metal was added to the resultant mixture and the sample was pelletized. The pellets were heated in evacuated quartz tubes at 1150°C for 2 weeks in a muffle furnace and slowly cooled (0.8–2° C/hr) to room temperature. Large single crystals were obtained by solid-state reaction only for the $m = 6$ and $m = 7$ members. Subsequently, partial substitution of potassium was carried out only on the $K_2P_8W_{24}O_{88}$ bronze by adding appropriate amounts of alkali metal carbonates (A_2CO_3 with A = Li, Na, Rb). For insertion reactions to form $K_2M_xP_8W_{24}O_{88}$ with M = Fe, Co, Sn, the appropriate metal oxides (FeO, CoO, SnO) were added to a stoichiometric mixture of DPTB. Similarly, the substitution of W by Mo was carried out by adding appropriate amounts of Mo powder to the $K_2P_8W_{24}O_{88}$ starting mixture.

The crystals were oriented by single

crystal X-ray diffraction techniques for the electrical transport measurements. Samples were identified by powder X-ray diffraction (PXD) using monochromatized Cu$K\alpha$ radiation on a Scintag PAD V diffractometer. Lattice parameters were determined by least-squares fitting of the observed PXD data. Si was used as an internal standard. Elemental analysis was determined by D.C. plasma emission spectroscopy.

Low-temperature resistivity (2–300 K) was measured using the standard four-probe configuration in a conventional cryostat with ultrasonically soldered indium contacts on the single crystals. Magnetic susceptibility was measured in a Quantum Design SQUID magnetometer from 4 to 250 K. A magnetic field of 1 T was employed to determine the susceptibilities along a^* and in the b^*c^* plane of the crystals.

Results and Discussion

Synthesis

Large, plate-like single crystals of $K_2P_8W_{24}O_{88}$ and $K_2P_8W_{28}O_{100}$ with an average size of $3 \times 1 \times 0.3$ mm^3 formed (Fig. 2) on the quartz tube surface surrounding the polycrystalline product. It is possible that the crystals grew as a result of partial melting of the polycrystalline product near the surface. Attempts to partially substitute for K^+ in polycrystalline $K_2P_8W_{24}O_{88}$ to form $K_{2-x}A_xP_8W_{24}O_{88}$ with $A = Li^+$, Na^+, and Rb^+ resulted in mixed alkali-metal single crystal $K_xA_yP_8W_{24}O_{88}$ ($x + y < 2$) and $K_{x'}A_{y'}P_8W_{24}O_{100}$ ($x' + y' < 2$) polycrystalline products as evidenced by chemical analysis and PXD. Efforts to prepare inserted $K_2M_xP_8W_{24}O_{88}$ with M = Fe, Co, Sn (x = 1.0) resulted in phases with only small amounts of M inserted (see Table I). The host, the mixed alkali metal $K_xA_yP_8W_{24}O_{88}$ (A = Li, Na, Rb), and the inserted $K_2M_xP_8W_{24}O_{88}$ (M = Fe, Sn, Co) bronzes form as dark, bluish, dichromic crystals

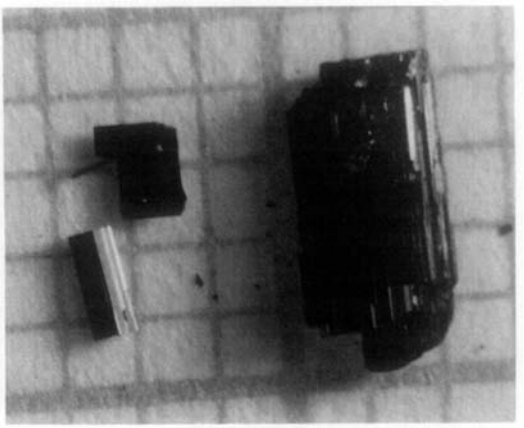

FIG. 2. Single crystals of $K_2P_8W_{24}O_{88}$.

TABLE I

ROOM TEMPERATURE RESISTIVITIES OF SELECTED POTASSIUM DIPHOSPHATE TUNGSTEN BRONZES AND THEIR SUBSTITUTED ANALOGS ALONG THE b (EASY DIRECTION) AND THE a^* (HARD DIRECTION) CRYSTALLOGRAPHIC AXES

Compound	ρ_b^{RT} (Ωcm)	$\rho_{a^*}^{RT}$ (Ωcm)
$K_2P_8W_{24}O_{88}$	1.2×10^{-4}	5.2×10^{-3}
$K_2P_8W_{23.94}Mo_{0.06}O_{88}$	1.8×10^{-4}	1.8×10^{-2}
$K_2P_8W_{22.70}Mo_{1.30}O_{88}$	1.1×10^{-4}	2.6×10^{-2}
$K_2P_8W_{22.28}Mo_{1.72}O_{88}$	1.0×10^{-3}	2.0×10^{-3}
$K_2P_8W_{28}O_{100}$	1.5×10^{-4}	8.9×10^{-3}
$K_2P_8W_{27.4}Mo_{0.6}O_{100}$	1.7×10^{-4}	2.7×10^{-2}
$K_2P_8W_{26.8}Mo_{1.2}O_{100}$	1.8×10^{-4}	2.1×10^{-2}
$K_2P_8W_{26.2}Mo_{1.8}O_{100}$	3.1×10^{-4}	[a]
$K_2P_8W_{23.8}Mo_{4.2}O_{100}$	1.0×10^{-3}	3.1×10^{-2}
$K_2Co_{0.08}P_8W_{24}O_{88}$	1.5×10^{-5}	[a]
$K_2Fe_{0.08}Sn_{0.10}P_8W_{24}O_{88}$	8.2×10^{-5}	3.5×10^{-3}
$K_2Sn_{0.2}P_8W_{24}O_{88}$	4.2×10^{-5}	2.6×10^{-3}
$K_{0.18}Li_{0.13}P_4W_{12}O_{44}$ [b]	3.2×10^{-5}	4.0×10^{-3}
$K_{0.53}Na_{0.42}P_4W_{12}O_{44}$ [b]	8.3×10^{-5}	6.7×10^{-3}
$K_{1.32}Rb_{0.28}P_8W_{24}O_{88}$	3.5×10^{-5}	8.8×10^{-3}

[a] Crystal is too small to attach contacts in the "hard" configuration.

[b] $MPTB_p$ (m = 6) structure; the easy direction of conductivity in $MPTB_p$ corresponds to the a crystal axis and the hard direction to the c axis of the orthorhombic unit cell.

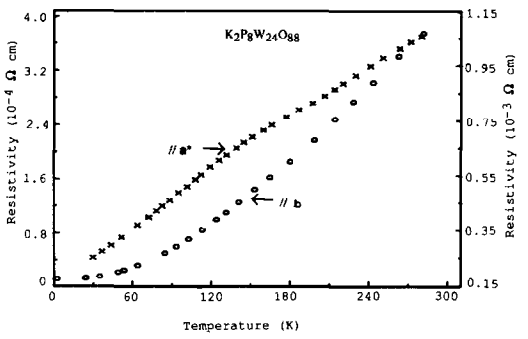

FIG. 3. Temperature dependence of the resistivity of a single crystal of $K_2P_8W_{24}O_{88}$ for current along the *b* (easy) and *a** (hard) crystal axes.

with golden edges. In the Mo-substituted $K_2P_8W_{24-x}Mo_xO_{88}$ crystals, the fringes gradually changed color from golden to copper with increasing Mo contents.

Properties of $K_2P_8W_{24}O_{88}$ and $K_2P_8W_{28}O_{100}$

The electrical resistivity was measured along the length, width, and depth of the bronze crystal plate. The length of the crystal plate was subsequently determined by single crystal X-ray techniques to correspond to the *b* crystallographic direction, while the depth and the width are along the *a** and *c** crystal axes, respectively. Room temperature resistivity values of selected crystals of various potassium diphosphate tungsten bronzes and their substituted analogs are summarized in Table I. For the hosts, $K_2P_8W_{24}O_{88}$ and $K_2P_8W_{28}O_{100}$, these values indicate quasi-2D behavior with the resistivity along *a** being one order of magnitude larger than the other two directions ($\rho_b \simeq \rho_c^*$). This is not surprising since the conduction paths (W–O–W) along *a** are interrupted by the insulating P_2O_7 groups (Fig. 1). Figures 3 and 4 show the temperature dependence of electrical resistivity along the easy (*b*) and hard (*a** which is approximately along the *a* axis) axes of conductivity for $K_2P_8W_{24}O_{88}$, and $K_2P_8W_{28}O_{100}$, respectively. The two bronzes show metallic and anisotropic behavior. The room temperature resistivities of $\rho_{a^*} \sim 10^{-3}$ and $\rho_b \sim 10^{-4}$ Ω cm are close to those observed in the hexagonal tungsten bronzes Na_xWO_3 (*1*), K_xWO_3 (*2*), and Rb_xWO_3 (*2*). However, the order–disorder anomaly seen in the resistivity of K_xWO_3 (*2*) ($0.18 < x < 0.32$) is not observed in these $DPTB_h$. This may be attributed to a different K^+ coordination configuration in the hexagonal tunnels of the $DPTB_h$ or to the fact that the K^+ ions are already ordered in these phosphate tungsten bronzes. It is possible that by varying the concentration of K^+ as in $K_xP_8W_{24}O_{88}$ the order–disorder phenomenon may be observed.

Figure 5 shows the temperature dependence of the magnetic susceptibility of $K_2P_8W_{24}O_{88}$ with the applied magnetic field (*H*) parallel with the *b* (easy direction) axis. The magnetic susceptibility is temperature independent, typical of Pauli paramagnetic behavior.

Properties of the Substituted and Inserted Phases of $K_2P_8W_{24}O_{88}$

As we have discussed above, attempts to form partially substituted phases of $K_{2-x}A_xP_8W_{24}O_{88}$ (A = Li, Na, Rb) resulted in single crystal $K_xA_yP_8W_{24}O_{88}$ ($x + y < 2$) and polycrystalline $K_{x'}A_{y'}P_8W_{28}O_{100}$ ($x' + y' < 2$) products. Both the single crystals

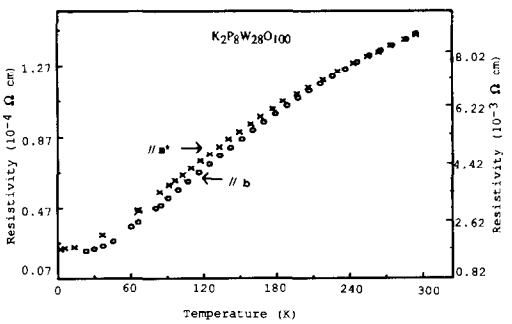

FIG. 4. Temperature dependence of the resistivity of a single crystal of $K_2P_8W_{28}O_{100}$ for current along the *b* (easy) and *a** (hard) axes.

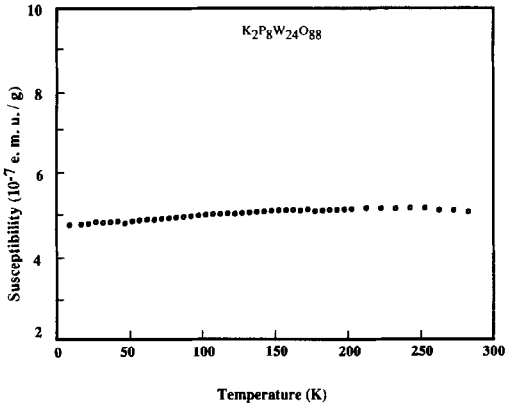

FIG. 5. Temperature variation of the magnetic susceptibility of a single crystal of $K_2P_8W_{24}O_{88}$. The applied magnetic field (H) is in the b^*c^* plane.

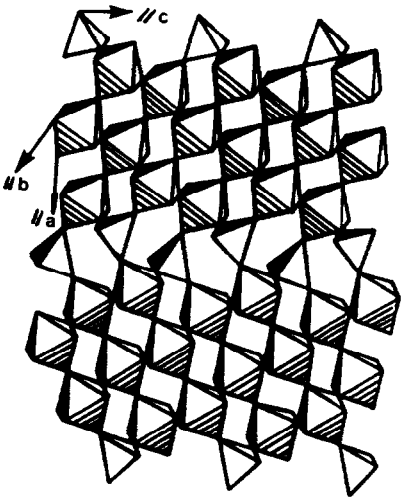

FIG. 6. Structure of $P_4W_{12}O_{44}$, monophosphate tungsten bronze with pentagonal tunnels $MPTB_p$ ($(PO_2)_4(WO_3)_{2m}$ with $m = 6$).

and polycrystalline phases form in the same reaction, but the K and A content of the poly- and single crystalline products are different according to our chemical analysis. It is likely that the poly- and single crystalline products form at different temperatures, because the crystals form at the surface of the pellets. All the polycrystalline samples form with the $K_2P_8W_{28}O_{100}$($DPTB_h$, $m = 7$) structure. The structure of the single crystals depends on the nature of the A cation: Rb substitution, as expected, has no effect on the structure of the $K_xRb_yP_8W_{24}O_{88}$ bronze since both $K_2P_8W_{24}O_{88}$ and $Rb_2P_8W_{24}O_{88}$ are known to have nearly identical structures (*5, 6*). However, when A = Li or Na, a $P_4W_{12}O_{44}$-like structure is observed. $P_4W_{12}O_{44}$ is the sixth member of the monophosphate tungsten bronze [$(PO_2)_4(WO_3)_{2m}$ with $m = 6$] forming with pentagonal tunnels, or $MPTB_p$ (see Fig. 6). The formation of $K_xA_yP_4W_{12}O_{44}$ in the $MPTB_p$ structure is very surprising since no $MPTB_p$ with partially occupied pentagonal tunnels had been synthesized previously by a solid-state reaction, although substantial lithium insertion into $MPTB_p$ using *n*-butyllithium (*n*-BuLi) at room temperature has been demonstrated (*13*). It is possible that at high temperatures, the $A_x(PO_2)_4(WO_3)_{2m}$ (A = K, Na) monophosphate tungsten bronze with hexagonal tunnels (henceforth the $MPTB_h$ structure (Fig. 7)) forms initially but, upon

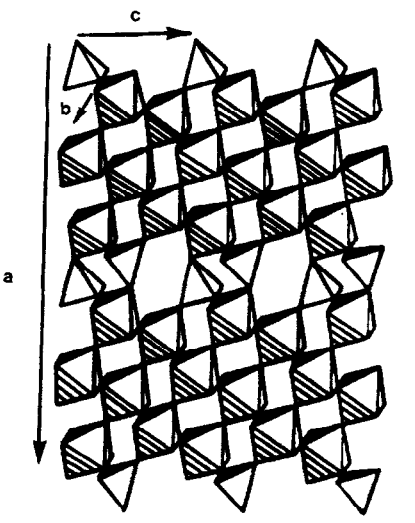

FIG. 7. Structure of $A_x(PO_2)_4(WO_3)_{2m}$ with A = K, Na, monophosphate tungsten bronze with hexagonal tunnels ($MPTB_h$).

prolonged heating at elevated temperature, the $MPTB_h$ structure transforms to the $MPTB_p$ structure, the stable phase at high temperature. The K^+ ion, because of its intermediate size between Na^+ and Rb^+ can lead to the $MPTB_h$ or the $DPTB_h$ structure. On the other hand, large cations such as Rb^+ lead to the $DPTB_h$ but not the $MPTB_h$ structure, while small cations such as Na^+ form only in the $MPTB_h$ structure. Interestingly, attempts to synthesize pure lithium phosphate tungsten bronzes with cations smaller than Na^+ (such as Li^+) have been unsuccessful so far, although insertion of Li^+ by *n*-BuLi into $DPTB_h$'s at low temperature is possible (*13*). However, $MPTB_p$'s with empty tunnels can be prepared. This suggests that Li–P–W–O bronzes are not stable, due possibly to the small size and large polarizing effect of the Li^+ ion, which would tend to contract the big cavities thereby collapsing the bronze lattice: lithium insertion reactions via *n*-BuLi show that the unit cell volumes of the lithiated phosphate tungsten bronze samples are smaller than those of the host bronzes (*13*).

Solid-state insertion reactions yield $K_2M_xP_8W_{24}O_{88}$ (M = Fe, Sn, Co) compounds with no observable structural changes relative to the host $DPTB_h$. Figure 8 shows the temperature dependence of resistivity along the *b* (easy axis) crystal axis of $K_xRb_yP_8W_{24}O_{88}$. (The Li and Na mixed alkali $K_xA_yP_4W_{12}O_{44}$ phases form a different structural type, i.e., $MPTB_p$, and comparison of their physical properties with the $DPTB_h$'s is inappropriate.) The positive coefficient of the temperature dependence of the resistivity indicates metallic behavior similar to that of the host $K_2P_8W_{24}O_{88}$ bronze. However, the conductivity along *b* in this bronze is about one order of magnitude higher than that of the host (Table I). Concomitantly, the anisotropy observed in $K_xRb_yP_8W_{24}O_{88}$ phases is significantly larger than that in the host bronze. A similar increase in the conductivity along the

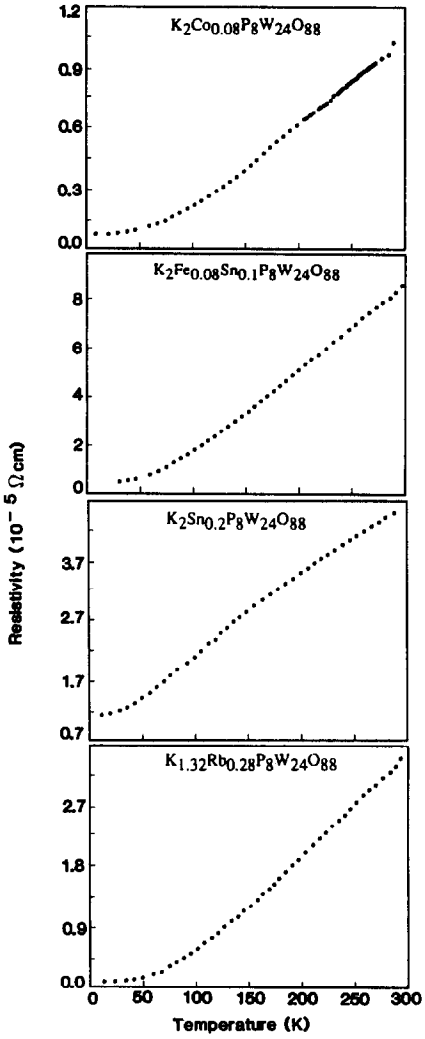

FIG. 8. Temperature dependence of the resistivity for $K_2M_xP_8W_{24}O_{88}$ with M = Fe, Sn, and Co, and $K_xRb_yP_8W_{24}O_{88}$ along the *b* axis.

b axis is observed in the resistivity of $K_2M_xP_8W_{24}O_{88}$ (M = Fe, Sn, Co) inserted bronze phases (Fig. 8). The magnetic susceptibilities of $K_xRb_yP_8W_{24}O_{88}$ and $K_2Sn_{0.2}P_8W_{24}O_{88}$ are comparable to those of the host (see Table II).

In $KP_8W_{40}O_{136}$ ($DPTB_h$ with m = 10) the W–O–W angle for crystallographically unique tungsten sites varies from 151° to

TABLE II

MAGNETIC SUSCEPTIBILITIES OF POTASSIUM DIPHOSPHATE TUNGSTEN BRONZES IN THE EASY (*bc*) PLANE

Compounds	$\chi_{bc}^{250\,K}$ (emu/g)
$K_2P_8W_{24}O_{88}$	5.0×10^{-7}
$K_2P_8W_{23.8}Mo_{4.2}O_{100}$	5.2×10^{-7}
$K_2Sn_{0.2}P_8W_{24}O_{88}$	5.2×10^{-7}
$K_{1.32}Rb_{0.28}W_{24}O_{88}$	1.7×10^{-7}

171° and the W–O distance varies from 1.71 to 2.06 Å along the *b* axis (*5*). By introduction of another alkali metal ion and/or a decrease in the number of alkali ions in $K_xRb_yP_8W_{24}O_{88}$ ($x + y < 2$) or insertion of ions such as Fe, Sn, or Co into available cavities in the lattice, the W–O–W angle might approach closer to 180°, and the extent of the W–O distance alternations might decrease, thereby improving conduction along the W–O–W linkages. If so, a systematic change in the *b* dimensions might be expected, but no change in *b* was observed as shown in Table III.

Mo substitution for W was studied in $K_2P_8W_{24-x}Mo_xO_{88}$ $0.04 < x \leq 4$. In these reactions both single crystal and polycrystalline products indicated intergrowth of $K_2P_8W_{24-x}Mo_xO_{88}$ and $K_2P_8W_{28-x}Mo_xO_{100}$ by powder X-ray diffraction. Some reactions lead to both polycrystalline and single crystal products of the $K_2P_8W_{24}O_{88}$ structure, and other reactions to the $K_2P_8W_{28}O_{100}$ structure. We found no clear correlation between the value of *x* and the particular structural type and/or intergrowth observed in the products.

In both $K_2P_8W_{24}O_{88}$ and $K_2P_8W_{28}O_{100}$, as the concentration of Mo increased, the temperature coefficient of the resistivity ($d\rho/$

TABLE III

LATTICE PARAMETERS OF SELECTED POTASSIUM PHOSPHATE TUNGSTEN BRONZES AND THEIR SUBSTITUTED ANALOGS

Compounds	*a* (Å)	*b* (Å)	*c* (Å)	β (°)	*V* (Å^3)
$K_2P_8W_{24}O_{88}$	14.03(5)	7.513(7)	17.05(2)	114.1(1)	1640(5)
$K_2P_8W_{23.94}Mo_{0.06}O_{88}$	14.04(2)	7.47(1)	16.99(8)	113.6(6)	1632(3)
$K_2P_8W_{22.70}Mo_{1.30}O_{88}$	14.05(1)	7.511(5)	16.91(4)	113.2(3)	1640(2)
$K_2P_8W_{22.28}Mo_{1.72}O_{88}$	14.09(1)	7.505(1)	16.87(1)	112.8(1)	1644(1)
$K_2P_8W_{28}O_{100}$	14.74(1)	7.526(1)	16.77(1)	99.66(7)	1833(1)
$K_2P_8W_{27.4}Mo_{0.6}O_{100}$	14.72(2)	7.509(4)	16.83(2)	99.50(14)	1834(2)
$K_2P_8W_{26.8}Mo_{1.2}O_{100}$	14.76(1)	7.521(1)	16.81(1)	99.40(5)	1841(2)
$K_2P_8W_{26.22}Mo_{1.78}O_{100}$	14.75(6)	7.514(3)	16.79(1)	99.34(5)	1837(2)
$K_2P_8W_{23.8}Mo_{4.2}O_{100}$	14.72(1)	7.505(2)	16.82(1)	99.65(3)	1832(1)
$K_2P_8Co_{0.08}W_{24}O_{88}$	14.02(1)	7.502(1)	17.22(2)	115.2(1)	1636(1)
$K_2Fe_{0.08}Sn_{0.10}P_8W_{24}O_{88}$	14.02(4)	7.556(10)	17.12(1)	114.5(1)	1651(1)
$K_2Sn_{0.2}P_8W_{24}O_{88}$	14.05(1)	7.513(3)	17.00(2)	113.7(1)	1644(1)
$K_{0.18}Li_{0.13}P_4W_{12}O_{44}$[a]	5.241(1)	6.600(1)	23.47(6)	90	814.2(2)
$K_{0.53}Na_{0.42}P_4W_{12}O_{44}$[a]	5.303(3)	6.581(5)	23.58(2)	90	823.4(7)
$K_{1.32}Rb_{0.28}P_8W_{24}O_{88}$	14.05(1)	7.516(6)	16.92(3)	113.2(3)	1642(3)
$K_{0.02}P_4W_{11.86}Mo_{0.14}O_{44}$[a]	5.317(1)	6.546(2)	23.64(3)	90	822.8(7)

[a] $MPTB_p$ ($m = 6$) structure.

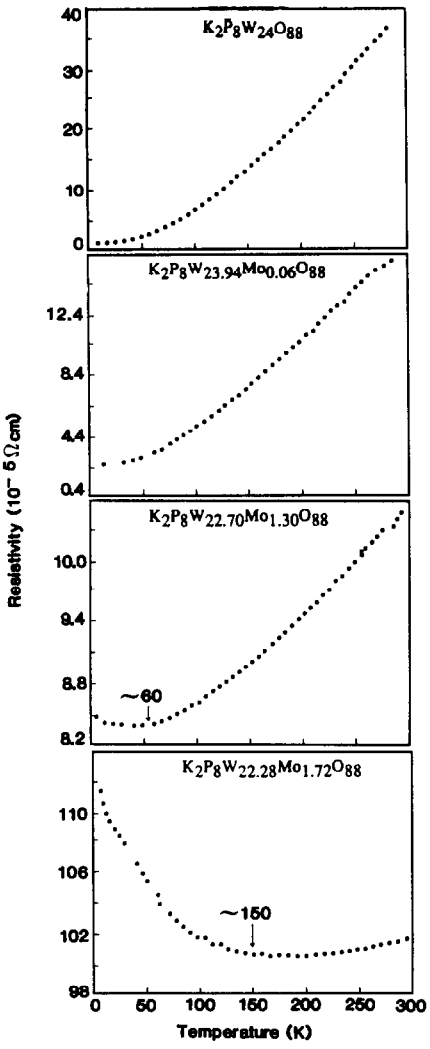

FIG. 9. Temperature variation of the resistivity of single crystals of $K_2P_8W_{24-x}Mo_xO_{88}$ along the *b* axis.

dT) decreased, and a broad metal–to–semiconductor transition developed gradually with increasing Mo content (Figs. 9 and 10). This decrease in the slope of the resistivity reflects a decrease in metallic character and is consistent with the interpretation that any interruption in the conduction paths, which consist of W–O–W linkages, would disrupt delocalization of *d* electrons and eventually result in electron localization. In the Mo-substituted $DPTB_h$ bronzes, the conduction paths are interrupted when Mo is substituted for W in the W–O–W link-

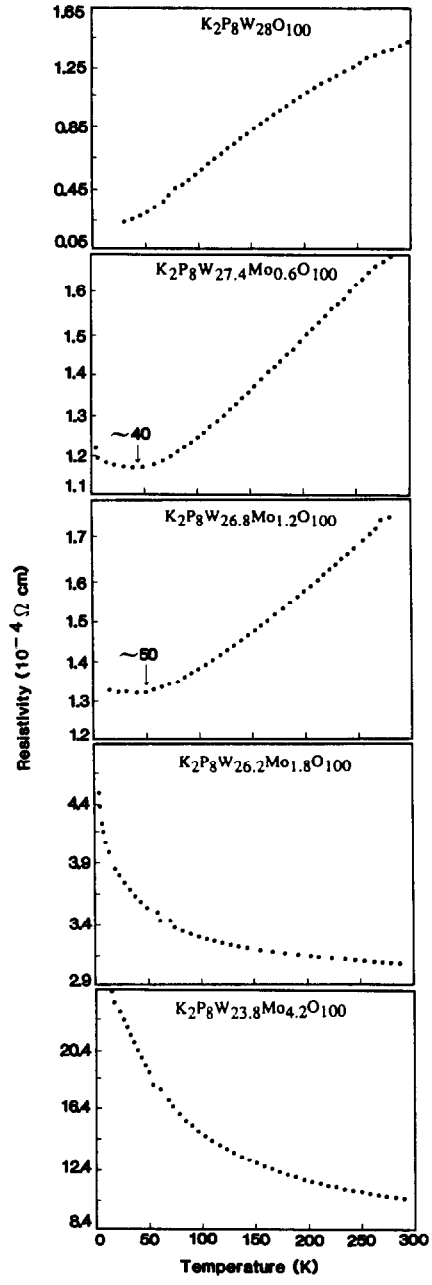

FIG. 10. Temperature variation of the resistivity of $K_2P_8W_{28-x}Mo_xO_{100}$ along the *b* axis.

ages. With increasing Mo content more localization is introduced, and the electronic properties change from metallic to semiconducting behavior. With respect to the host bronzes, there is about one order of magnitude increase in the anisotropy of the Mo-substituted $DPTB_h$, which is due largely to a decrease in the conductivity along the a^* direction (Table I). The critical concentration of Mo at which the $K_2P_8W_{24-x}Mo_xO_{88}$ and $K_2P_8W_{28-x}Mo_xO_{100}$ bronzes become semiconducting are $x > 1.3$ and $x = 1.2$, respectively.

Band Electronic Structures

Figure 11 shows the dispersion relations of the bottom portion of the t_{2g}-block bands calculated for the $W_{24}O_{84}$ slab found in $Rb_{1.8}P_8W_{24}O_{88}$, where the dashed line refers to the Fermi level appropriate for $K_2P_8W_{24}O_{88}$. The Fermi level cuts six dispersive bands along $\Gamma \rightarrow Y$, two along $\Gamma \rightarrow Z$, four along $Z \rightarrow M$, and two along $M \rightarrow Y$. Thus, the band structure of the $W_{24}O_{84}$ slab consists of not only one- but also two-dimensional character. However, more bands are cut by the Fermi level along the b direction (i.e., $\Gamma \rightarrow Y$ and $Z \rightarrow M$), so that the electrical conductivity is expected to be greater along the b axis than along the c axis. This expectation is consistent with our resistivity measurements on $K_2P_8W_{24}O_{88}$. Figure 12 shows the dispersion relations of the bottom portion of the t_{2g}-block bands calculated for the $W_{28}O_{96}$ slab found in $Rb_{1.74}P_8W_{28}O_{100}$. As in the case of the $W_{24}O_{84}$ slab, the band electronic structure of the $W_{28}O_{96}$ slab consists of both one- and two-dimensional character, and the electrical conductivity is expected to be greater along the b axis than along the c axis. These are consistent with our resistivity measurements on $K_2P_8W_{28}O_{100}$.

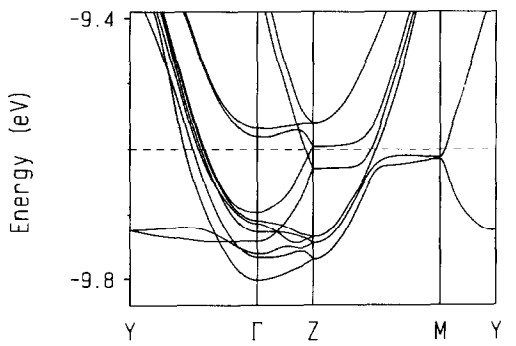

FIG. 11. Dispersion relations of the bottom portion of the t_{2g}-block bands calculated for the $W_{24}O_{84}$ slab, where $\Gamma = (0, 0)$, $Y = (b^*/2, 0)$, $Z = (0, c^*/2)$, $M = (b^*/2, c^*/2)$. The dashed line is the Fermi level appropriate for $K_2P_8W_{24}O_{88}$.

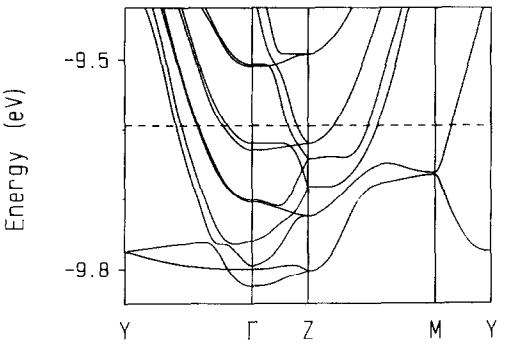

FIG. 12. Dispersion relations of the bottom portion of the t_{2g}-block bands calculated for the $W_{28}O_{96}$ slab, where $\Gamma = (0, 0)$, $Y = (b^*/2, 0)$, $Z = (0, c^*/2)$, and $M = (b^*/2, c^*/2)$. The dashed line is the Fermi level appropriate for $K_2P_8W_{28}O_{100}$.

It should be noted from Fig. 11 that there are flat bands above and slightly below the Fermi level in the $Z \rightarrow M$ region. Such bands give rise to a large density of states (DOS). Thus, the DOS value at the Fermi level, i.e., $n(e_f)$, can be increased if the Fermi level is either lowered or raised to those flat band regions. Such an increase in $n(e_f)$ may be responsible for the observed increase in the conductivity seen for both the $K_xA_yP_8W_{24}O_{88}$ ($x + y < 2$, i.e., electron deficient) and $K_2M_xP_8W_{24}O_{88}$ ($x > 0$, i.e., electron rich) systems. In fact, our calculations for $K_{1.32}Rb_{0.28}P_8W_{24}O_{88}$ and $K_2Sn_{0.2}P_8W_{24}O_{88}$ show that their Fermi levels lie in the flat band regions. In Fig. 12, flat bands are present slightly below and

well above the Fermi level. Thus, only electron-deficient samples $A_{2-x}P_8W_{28}O_{100}$ ($x > 0$) are expected to show conductivity increase.

Concluding Remarks

Temperature dependence of the electrical resistivity and magnetic susceptibility of oriented crystals of the diphosphate tungsten bronzes $K_2P_8W_{24}O_{88}$ and $K_2P_8W_{28}O_{100}$ show metallic and anisotropic properties consistent with their quasi-two-dimensional structures. A gradual change from metallic to semiconducting behavior is observed with increasing substitution of Mo for W.

Inserted bronze phases $K_2M_xP_8W_{24}O_{88}$ (M = Fe, Sn, Co) with $x \leq 0.2$ show a marked decrease of resistivity along the b crystallographic axis, the easy direction of conductivity. Similar behavior in electronic properties is observed in partially substituted $K_xRb_yP_8W_{24}O_{88}$ bronzes. The electrical resistivity observed for both the inserted and the partially substituted bronzes is remarkably low (10^{-5} Ω cm). Indeed, these materials are very good metals. The temperature dependence of the magnetic susceptibilities of the host bronzes and the substituted and inserted phases show Pauli paramagnetic behavior consistent with their metallic properties. All these observations are well accounted for by the band electronic structures of the $W_{24}O_{84}$ and $W_{28}O_{96}$ slabs. For $K_xA_yP_8W_{24}P_{88}$ with A = Li and Na, a transition from the diphosphate tungsten bronze ($DPTB_h$) structure of $K_2P_8W_{24}O_{88}$ to the monophosphate tungsten bronze ($MPTB_p$) structure of $P_4W_{12}O_{44}$ is observed.

Acknowledgments

This research was supported by the National Science Foundation–Solid State Chemistry Grants DMR-84-04003, DMR-87-14072 and the National Science Foundation Materials Research Instrumentation Grants DMR-84-08266, DMR-87-05620. Work at the Université de Paris-Sud and North Carolina State University was supported by the NATO, Scientific Affairs Division, and also by DOE, Office of Basic Sciences, Division of Materials Science under Grant DE-FG05-86ER45259.

References

1. P. A. Lightsey, D. A. Lilienfield, and D. F. Holcomb, *Phys. Rev. B* **14,** 4730 (1976).
2. L. H. Cadwell, R. C. Morris, and W. G. Moulton, *Phys. Rev. B* **23,** 2219 (1981).
3. R. K. Stanley, R. C. Morris, and W. G. Moulton, *Phys. Rev. B* **20,** 1903 (1979).
4. R. K. Stanley, R. C. Morris, and W. G. Moulton, *Phys. Rev. B* **20,** 3670 (1979).
5. M. Hervieu and B. Raveau, *J. Solid State Chem.* **43,** 291 (1982).
6. J. P. Giroult, M. Goreaud, Ph. Labbe, and B. Raveau, *Acta Crystallogr. B* **38,** 2342 (1982).
7. J. P. Giroult, M. Goreaud, Ph. Labbe, J. Provost, and B. Raveau, *Mater. Res. Bull.* **16,** 811 (1981).
8. M. Lamire, Ph. Labbe, M. Goreaud, and B. Raveau, *J. Solid State Chem.* **71,** 342(1987).
9. M.-H. Whangbo and R. Hoffmann, *J. Amer. Chem. Soc.* **100,** 6093 (1978).
10. J. P. Giroult, M. Goreaud, Ph. Labbe, and B. Raveau, *Acta Crystallogr. B* **37,** 1163 (1981).
11. R. Hoffmann, *J. Chem. Phys.* **39,** 1397 (1963). A modified Wolfsberg-Helmhotz formula was used to calculate the off-diagonal H_{ij} values: see, J. H. Ammeter, H.-B. Burgi, J. Thibeault, and R. Hoffmann, *J. Amer. Chem. Soc.* **100,** 3686 (1978).
12. E. Wang, M. Greenblatt, I. E.-I. Rachidi, E. Canadell, and M.-H. Whangbo, *Inorg. Chem.*, in press.
13. E. Wang and M. Greenblatt, *J. Solid State Chem.* **68,** 38 (1987).